2-Hydroxyoleate, a nontoxic membrane binding anticancer drug, induces glioma cell differentiation and autophagy

Silvia Terés[a,1], Victoria Lladó[a,1], Mónica Higuera[a,1], Gwendolyn Barceló-Coblijn[a], Maria Laura Martin[a], Maria Antònia Noguera-Salvà[a], Amaia Marcilla-Etxenike[a], José Manuel García-Verdugo[b], Mario Soriano-Navarro[b], Carlos Saus[a], Ulises Gómez-Pinedo[c], Xavier Busquets[a], and Pablo V. Escribá[a,2]

[a]Molecular Cell Biomedicine, Department of Biology-Institut Universitari d'Investigacions en Ciències de la Salut, University of the Balearic Islands, 07122 Palma de Mallorca, Spain; [b]Laboratorio de Morfología Celular, Unidad Mixta Centro de Investigación Príncipe Felipe-Universitat de València Estudi General, Centro de Investigación Biomédica en Red, Enfermedades Neurodegenerativas, 46013 Valencia, Spain; and [c]Laboratory of Regenerative Medicine, Neuroscience Institute, Hospital Clínico San Carlos, 28040 Madrid, Spain

Edited by* John E. Halver, University of Washington, Seattle, WA, and approved April 4, 2012 (received for review November 9, 2011)

Despite recent advances in the development of new cancer therapies, the treatment options for glioma remain limited, and the survival rate of patients has changed little over the past three decades. Here, we show that 2-hydroxyoleic acid (2OHOA) induces differentiation and autophagy of human glioma cells. Compared to the current reference drug for this condition, temozolomide (TMZ), 2OHOA combated glioma more efficiently and, unlike TMZ, tumor relapse was not observed following 2OHOA treatment. The novel mechanism of action of 2OHOA is associated with important changes in membrane-lipid composition, primarily a recovery of sphingomyelin (SM) levels, which is markedly low in glioma cells before treatment. Parallel to membrane-lipid regulation, treatment with 2OHOA induced a dramatic translocation of Ras from the membrane to the cytoplasm, which inhibited the MAP kinase pathway, reduced activity of the PI3K/Akt pathway, and downregulated Cyclin D-CDK4/6 proteins followed by hypophosphorylation of the retinoblastoma protein (RB). These regulatory effects were associated with induction of glioma cell differentiation into mature glial cells followed by autophagic cell death. Given its high efficacy, low toxicity, ease of oral administration, and good distribution to the brain, 2OHOA constitutes a new and potentially valuable therapeutic tool for glioma patients.

fatty acids | sphingomyelin synthase | cancer drug target | glioma biomarker

Cancer cells of undifferentiated phenotype (e.g., glioma) have a poor prognosis and limited treatment options. Primary brain tumors, of which glioma is the most common, are generally associated with very high rates of mortality (*ca.* 90%), being the median survival of patients about 1 y (1, 2). Chemotherapy provides only modest benefits to radiotherapy and surgery being the alkylating agent temozolomide (TMZ) the reference drug; however, tumor relapse is usually observed, and TMZ only increases the patients' life expectancy about 2.5 m (from 12.1 to 14.6 m: ref. 3). The present study was designed to investigate the efficacy of 2OHOA against glioma and its molecular mechanisms of action. 2OHOA exhibited a greater efficacy than TMZ in the treatment of glioma, and there was no relapse after long-term treatment with 2OHOA. This efficacy and lack of toxicity at therapeutic doses has been acknowledged recently by the European Medicines Agency (EMA) to designate 2OHOA orphan drug for the treatment of glioma. In previous studies, we showed that this compound induces cell cycle arrest of lung cancer cells (4–6). Here, we showed that 2OHOA reversed the altered lipid profile of glioma cells and how this modification regulated cell signaling to induce autophagy specifically in glioma but not normal cells.

Moreover, in the present study we demonstrated that the changes induced by 2OHOA were specific to cancer cells with no significant effects observed in normal cells and no adverse effects in treated animals, features not shared by most anticancer drugs. The efficacy of this compound in the absence of any relevant toxicity indicates that 2OHOA may be a useful and innovative therapeutic tool to treat glioma.

Results

Efficacy of 2OHOA and TMZ Against Glioma. The efficacy of 2OHOA against glioma was tested in the human glioma cell lines SF767, U118, A172, and T98G. In these lines, 2OHOA induced a time and concentration dependent inhibition of cell growth (Fig. 1*A* and Fig. S1*A*). Likewise, TMZ induced inhibition of human SF767 glioma cell growth, but it failed to kill all the cancer cells in culture exhibiting a lower efficacy in this model of human glioma than 2OHOA.

In a xenograft model of human glioma (SF767 cells), 2OHOA was also more potent than TMZ (Fig. 1*B*). This effect was dose dependent being the sodium salt more potent than other forms of 2OHOA (Fig. S1*B*); therefore, it was used throughout this work. In this context, the combined treatment with both was more efficient than either alone possibly because their different modes of action (600 mg/kg 2OHOA and/or 80 mg/kg TMZ, p.o., daily, 50 d: Fig. 1*B*). To determine possible tumor relapse after treatment, both compounds were assessed for a further 21 d after 60 d treatments. Following TMZ treatment, the tumors derived from human glioma SF767 cells again grew in an aggressive manner (Fig. 1*B*). Similar results have been reported in patients with glioma in whom TMZ treatment only increases median survival by 10 wk (3, 7, 8). In contrast, tumor relapse was not observed after 2OHOA treatment (Fig. 1*B*). Using an orthotopic model of human glioma, oral administration of 2OHOA completely eliminated glioma cell tumors in the brain of three mice and, in the other two, only a few SF767 cells remained (Fig. 1*C* and Fig. S1*C*). In this context, HuNu+ (i.e., human glioma) cells were in the vicinity of the ventricle with some labeling on the choroid plexus. In animals treated with TMZ, a reduction of the tumor size was also observed; though, the size of tumors and their immunoreactivity were greater than in animals treated with 2OHOA (Fig. 1 and Fig. S1).

Author contributions: P.V.E. designed research; S.T., V.L., M.H., G.B.-C., M.L.M., M.A.N.-S., A.M.-E., M.S.-N., C.S., U.G.-P., and X.B. performed research; S.T., J.M.G.-V., and P.V.E. analyzed data; and P.V.E. wrote the paper.

The authors declare no conflict of interest.

*This Direct Submission article had a prearranged editor.

[1]S.T., V.L., and M.H. contributed equally to this work.

[2]To whom correspondence should be addressed. E-mail: pablo.escriba@uib.es.

This article contains supporting information online at www.pnas.org/lookup/suppl/doi:10.1073/pnas.1118349109/-/DCSupplemental.

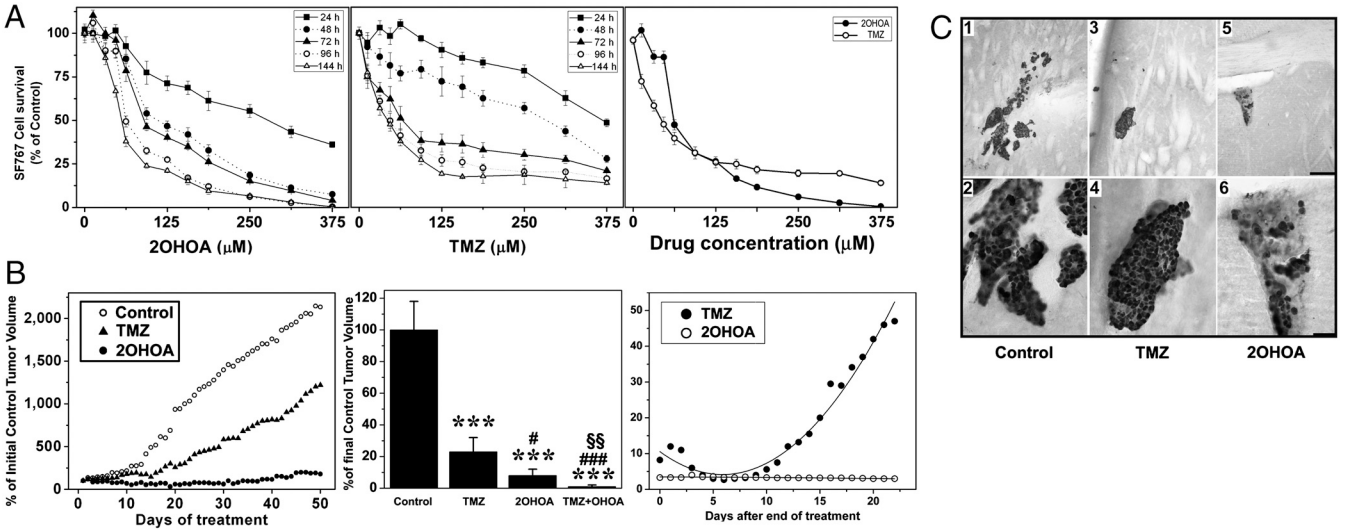

Fig. 1. Efficacy of 2OHOA against human glioma (SF767) cells and tumors. (*A*) Time and concentration dependent inhibition of human glioma (SF767) cell growth by 2OHOA (*left*), TMZ (*center*), and their compared efficacy at 96 h (*right*, $N = 6$–8). (*B*) Effects of vehicle (control), 2OHOA, TMZ or both against SF767-derived tumor growth in mice during 50 d treatments (*left*, $N = 20$), 60-d treatments (center, $N = 15$), and tumor volumes during 3 wk following 60 d treatments (*right*). ***$P < 0.001$ with respect to control; #, $P < 0.05$, ###, $P < 0.001$ with respect to TMZ alone; §§, $P < 0.01$ with respect to 2OHOA or TMZ alone. (*C*) Effects of vehicle (1, 2), TMZ (3, 4), and 2OHOA (5, 6) on orthotopic human glioma growth (SF767 cells) in the brain of nude mice after 42 d treatments ($N = 5$). Additional pictures are shown in Fig. S1. In all cases, the doses were 600 mg/kg for 2OHOA and 80 mg/kg for TMZ (p.o., daily). Scale bars = 200 μm (1, 3, 5) and 50 μm (2, 4, 6).

2OHOA Regulates Glioma Membrane-Lipid Composition and Structure. 2OHOA is a synthetic fatty acid that readily binds to the plasma membrane and regulates its lipid structure (4, 9). It induces important changes in the membrane structure that favor the binding of certain proteins like protein kinase Cα (PKCα: 4, 9). 2OHOA was detected in SF767 cell membranes as a free fatty acid (*ca.* 7%) or incorporated in phospholipids (*ca.* 30%), constituting a major membrane fatty acid upon treatment. In addition, significant alterations in the levels of various membrane lipids were observed after 2OHOA treatment including marked increases in SM (*ca.* 2-fold: Fig. 2) and 1,2-diacylglycerol (DAG, from 2.05 ± 0.17 in untreated cells to 3.02 ± 0.11 nmole/mg protein in 2OHOA-treated cells) and marked decreases in phosphatidylethanolamine (PE) mass (Fig. 2). No such changes were observed following 2OHOA treatment of normal (MRC-5) cells (Fig. 2 and Fig. S2) that already exhibit high basal levels of SM. The increase in DAG and the presence of 2OHOA itself favors the cytosol to membrane translocation and activation of PKCα (4, 10) that is associated with knockdown of E2F-1 and DHFR (5, 6). The increase in membrane 2OHOA was likely associated with short-term (10 min) Ras release from the membrane and the subsequent inhibition of the ERK pathway, and changes in SM and PE could be related the long-term Ras translocation (Fig. 3 and Fig. S3).

2OHOA Inhibits the EGFR/Ras/MAP Kinase and PI3K/Akt Pathways in Glioma cells. The EGFR/Ras/MAP kinase and PI3K/Akt pathways are usually hyperactive and cause proliferation and loss of differentiation in glial cells (11–14). Treatment with 2OHOA, which induced changes in the membrane-lipid composition of glioma cells, caused translocation of Ras from the plasma membrane to the cytoplasm (the perimembranal content of Ras determined by confocal microscopy changed from $87 \pm 6\%$ to $6 \pm 3\%$ in the absence or presence of 2OHOA); but, it did not significantly change the total cellular Ras content ($98.6 \pm 4.4\%$ and $94.7 \pm 6.2\%$ in control and 2OHOA-treated cells, as determined by immunoblotting: Fig. S4). Ras propagates incoming messages from membrane growth factor receptors (e.g., EGFR) to downstream proteins such as Raf at defined l_d lipid microdomains in the plasma membrane (15, 16). As such, its translocation to the cytoplasm greatly affected the proliferative Ras/MAPK signaling, which is frequently overactive in cancer cells and responsible for their loss of differentiation (17, 18). Indeed, a significant reduction in the levels of phospho-EGFR and phosphorylated (i.e., active) cRaf, MEK and MAP kinases (ERK1 and ERK2) was observed in vitro (SF767 cells) and in vivo (tumors) after 2OHOA treatments (Fig. 3, and Figs. S3 and S4). No significant changes in the levels of total Raf, MEK, or ERK were observed (Fig. S4). The PI3K/Akt signaling pathway is involved in cell survival and growth in

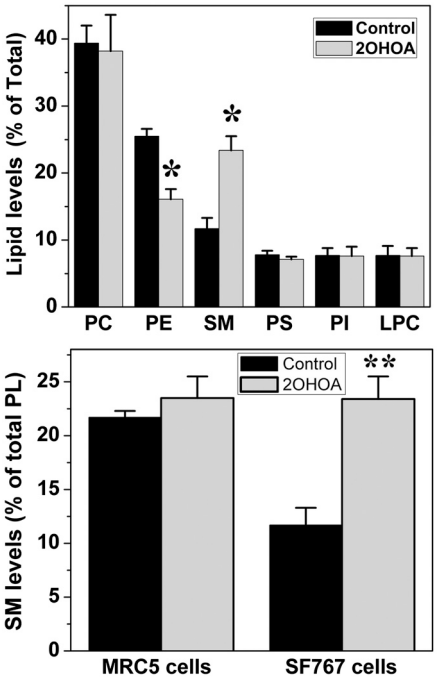

Fig. 2. 2OHOA (72 h, 200 μM) induces changes in SF767 membrane-lipid composition. *Upper panel*, Levels of the major phospholipid classes before (black bars) and after (gray bars) 2OHOA treatment: PC, phosphatidylcholine; PE, phosphatidylethanolamine; SM, sphingomyelin; PS, phosphatidylserine; PI, phosphatidylinositol; LPC, lyso-phosphatidylcholine. *Lower panel*, effects of 2OHOA (72 h, 200 μM) on SM levels in normal (MRC5) and glioma (SF767) cells before (black) and after (gray) treatment ($N = 6$–8).

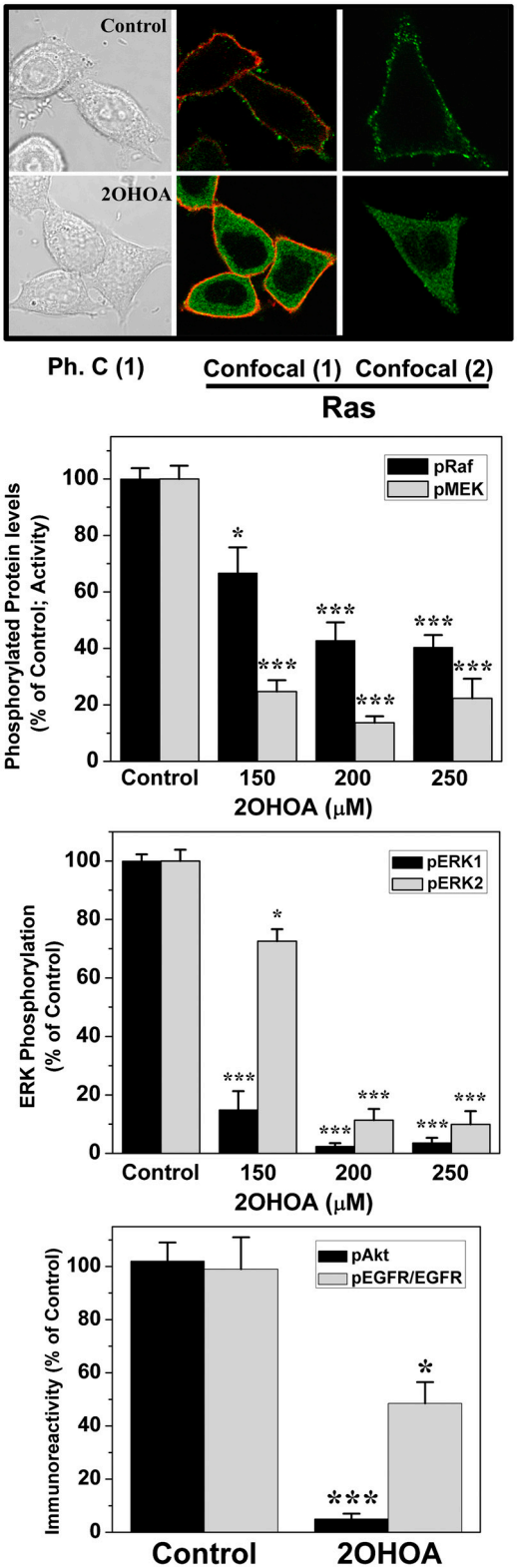

Fig. 3. Effect of 2OHOA on the MAPK (ERK) and PI3K/Akt pathways in SF767 cells. *Top*: 2OHOA (150 μM) induces Ras (green fluorescence) translocation from the membrane to the cytoplasm after incubations of 10 min (1) or 24 h (2). Ph. C.: phase contrast micrography. In confocal micrographies, the red fluorescence corresponds to the membrane labeling as detected with the raft marker Vybrant Alexa Fluor 594 (Molecular Probes). Effects of 2OHOA (0, 150, 200, and 250 μM) on the phosphorylation (i.e., activity) of Raf (*second panel*), MEK and ERK1/2 (*third panel*), and EGF-stimulated Akt and EGFR phosphorylation (150 μM, 12 h after a 15 min stimulation with 35 ng/ml EGF; *bottom panel*). $N = 6$–8 in all cases.

cooperation with the Ras/MAPK pathway in cancer cells (17). Following 2OHOA treatment, we observed a significant reduction in Akt phosphorylation indicating that this protein is preferentially inactive (Fig. 3).

2OHOA Induces Cell Cycle Arrest in Human Glioma Cells. Cell cycle arrest has been shown to occur in response to PKC activation in various cancer cell types (4–6, 19, 20). In human glioma cells, we have seen that 2OHOA induced a rapid (minutes) and sustained (over 24 h) activation (translocation to membrane) of PKC that caused overexpression of $p21^{Cip1}$ and a simultaneous increase of $p27^{Kip1}$ (Fig. S5). These potent CDK inhibitors (CDKIs, ref. 21) are frequently downregulated in gliomas, and their rise induced decreases of Cyclin D1, Cyclin D3, and CDK4 and CDK6 that caused RB hypophosphorylation, E2F-1 downregulaiton and DHFR knockdown (Fig. S5) followed by cell cycle arrest in $G_{0/1}$ of glioma cells. No significant changes in the levels of these proteins were seen in MRC-5 cells (immunoreactivities for these proteins were 91–112% for all these proteins being $P > 0.05$ always).

2OHOA Induces Human Glioma Cell Differentiation. In addition to their increased proliferation, glioma cells lose many molecular and morphological features of differentiated glial cells such as the typical stellar shape and the expression of glutamine synthetase (GS) and glial fibrillary acidic protein (GFAP; 22, 23). It has been proposed that inducing differentiation may be a suitable approach to treat cancer given its potential specificity and low level of toxicity (24). In this context, treatment with 2OHOA induced a marked differentiation of glioma cells resulting in the recovery of the stellar morphology of mature astrocytes and the expression (in vitro and in vivo) of the glial differentiation markers GFAP and GS, in SF767 cells (Fig. 4). Because the final effect of 2OHOA was induction of autophagy, it could be feasible

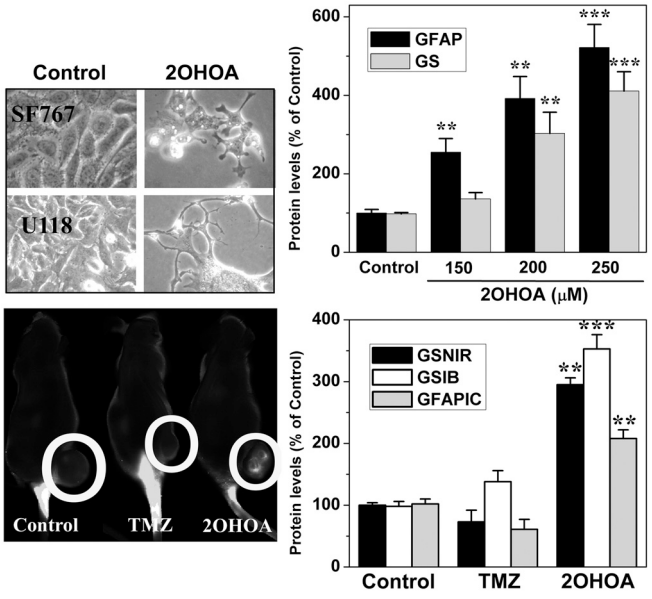

Fig. 4. 2OHOA induces glioma cell differentiation in vitro and in vivo. *Top*, phase contrast micrographs of SF767 and U118 (human glioma) cells maintained in the presence or absence (control) of 2OHOA for 72 h (*Left*, 200 μM, 200x magnification). 2OHOA induced the expression of GFAP and GS (*right*) in SF767 cells as determined in immunoblots. *Bottom*, In vivo near infrared detection of a fluorolabeled anti-GS antibody in nude mice with SF767-derived tumors following treatment with the vehicle lone (control), 2OHOA and TMZ (*Left*, $N = 10$ per group) and the corresponding quantification (*Right*, GSNIR, mean ± SEM). GS was also determined ex vivo in these animals using immunoblotting (GSIB). GFAP was also quantified by immunocytochemistry (GFAPIC, *Right*).

that redifferentiation may lead to the initiation of death programs in cancer cells, though this point requires further studies.

2OHOA Induces Glioma Cell Autophagy. 2OHOA treatment resulted in the death of the majority of cells in tumors derived from SF767 cells (Fig. 5 and Fig. S6). Similarly, in cultured SF767 cells, long-term (120 h) incubation with 2OHOA induced important morphological alterations that were observed in semithin sections (1.5 μm) by optical microscopy and thin (0.06–0.09 μm) sections by electron microscopy (Fig. 5). Thus, optical microscopy images revealed that untreated cells were oval in shape, with nuclei containing multiple nucleoli distributed along the nuclear matrix and few invaginations. In contrast, 2OHOA-treated cells (120 h, 300 μM) exhibited irregular morphology and were markedly smaller. Their nuclei were also smaller and contained deep invaginations whose depth was concentration dependent (Fig. 5). Notably, 2OHOA induced the appearance of lipid droplets and dense bodies, the latter scattered throughout the cytoplasm and some exhibiting morphological characteristics of autophagosomes (Fig. 5). At low and high 2OHOA concentrations, a loss of ER cisternae was observed in the cytoplasm consistent with the autophagic process (Fig. 5).

In turn, the unspecific ER stress inducer palmitic acid caused similar autophagosome synthesis induction in SF767 and MRC-5 cells (Fig. S6*B*). Finally, the expression of the autophagosome proteins LC3B and ATG5 increased significantly in a time and concentration dependent manner in SF767 cells (Fig. 5).

Discussion

In this study, the efficacy of the synthetic fatty acid 2OHOA in the treatment of glioma was demonstrated, and its mode of action

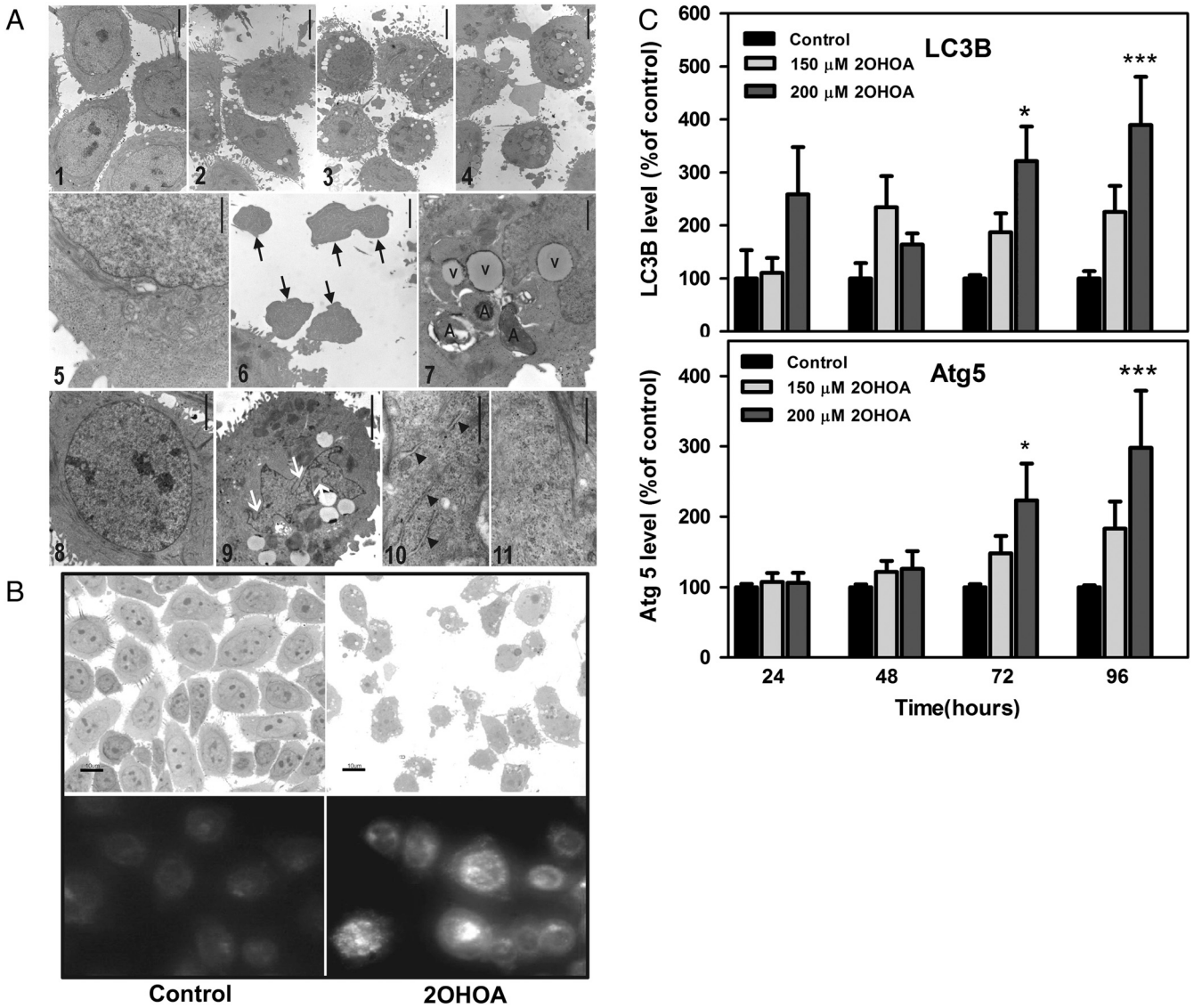

Fig. 5. (*A*) Electron microscopy of SF767 cells maintained for 120 h in the presence or absence (control, *panels 1, 5, 8, and 10*) of 2OHOA (100 μM: *panel 2*; 200 μM: *panels 3, 6*, and *7*; 300 μM: *panels 4, 9* and *11*). Arrows in *panel 6* correspond to SF767 fragments. In *panel 7*, V corresponds to lipid vesicles and A accounts for autophagosomes. The nuclei of SF767 cells cultured in the presence (*panel 9*) or absence (*panel 8*) of 2OHOA are shown, and the white arrows correspond to nuclear invaginations (bar = 2.5μm). 2OHOA treatment caused loss of rough endoplasmic reticulum cisternae in 2OHOA-treated cells (*panel 11*) compared with control cells (*panel 10*, arrows show cisternae; bar = 0.5 μm). $N = 300$ for each concentration and time used. (*B*) *Upper panels*, optical microscope photographs (1.5 μm semithin sections) showing SF767 cells treated for 120 h with vehicle (control) or 2OHOA (300 μM). *Bottom panels*, Fluorescence of lysosome/autophagosome labeled with Lysosensor in SF767 cells in the presence or absence (*left*) of 2OHOA (150 μM for 48 h, right). $N = 400$ cells from five independent experiments. The relative fluorescence was quantified using the Image J 1.38x software, and data are indicated in the Results section. (*C*) Effect of 2OHOA (150 μM and 200 μM) at different times (24–96 h) on the markers of autophagy, LC3B (*upper panel*) and Atg5 (*lower panel*).

described, driving glioma-to-glial cell differentiation that was followed by autophagy through the specific inhibition of the Ras-MAPK, Cyclin/CDK-DHFR, and PI3K-Akt pathways. 2OHOA is more efficient drug against human glioma than TMZ, the current reference drug to treat this condition. Unlike TMZ, no tumor relapse was observed following 2OHOA treatment (Fig. 1). Its low toxicity (IC_{50} > 5,000 μM, in normal MRC5 cells, and minimum lethal dose >3,000 mg/kg in rats) is unusual for anticancer drugs further supporting the specificity of 2OHOA and its use as differentiation therapy agent to treat cancer (24). Based on these facts, the EMA has acknowledged the potential significant benefit of 2OHOA and has recently designated this molecule an orphan drug for the treatment of glioma.

The plasma membrane contains thousands of different lipids that form various types of membrane microdomains that can be differentially and specifically regulated by drugs targeting the lipid bilayer. Thus, membrane-lipid therapy aims at the specific regulation of certain membrane-lipid structures to treat cancer and other human pathologies (25). In this context, very low levels of SM were found in human glioma (SF767) cells when compared with normal (MRC-5) cells, a characteristic common to all the cancer cell lines that we have studied to date (leukemia, lung cancer, and other glioma cells; ref. 26). In SF767 cells, 2OHOA treatments induced restoration of SM to levels similar to those observed in nontumor cells (Fig. 2). This observation (along with other results shown here) suggests that lower SM levels in cancer cells could facilitate high Ras-MAPK activity to express the malignant phenotype. The bulky isoprenyl moiety of Ras proteins can be anchored in membrane domains with high content of PE whereas it is excluded from SM-rich domains where the dense surface membrane packing prevents isoprenyl binding. Thus, Ras translocation to the cytoplasm (Fig. 3) was probably caused by changes in membrane lipids induced by 2OHOA, which could impair productive interactions between EGFR and Ras and Ras and Raf at the plasma membrane, and finally inactivate the MAPK cascade (protein expression was not altered). In fact, tipifarnib and other farnesyl transferase inhibitors exert their anticancer effects impairing Ras binding to membranes by blocking Ras isoprenylation (27). Therefore, the presence of 2OHOA first and the normalization of SM and PE levels, later induced changes in the membrane-lipid structure that caused recovery of the localization and activity of relevant signaling proteins (Fig. 2, and Figs. S2 and S3), which constitutes an alternative approach for the treatment of cancer (28). In this context, the regulation of SM levels by 2OHOA (via activation of sphingomyelin synthetase, ref. 26) is crucial in its mechanism of action against glioma. In line with these results, the addition of SM to culture medium enhances gemcitabine-mediated pancreatic cancer cell death (29) further indicating the relevance of this lipid in cancer cell survival. On the other hand, 2OHOA treatments induced specific changes in the levels of other membrane lipids (DAG, PE, and 2OHOA) that contributed to remodel membrane microdomains and regulated glioma cell signaling (30–32). These changes also facilitated the membrane binding and activation of PKCα (4, 10, and Fig. S5) that, itself, triggers inhibitory effects against cancer cell growth (4, 19, 20, and Fig. 5).

The canonical signaling cassette made up of EGFR, Ras, Raf, MEK, and ERK and/or the PI3K/Akt signaling pathway are overactivated in most human gliomas as well as in other types of cancer, and they often cooperate to induce malignant transformation of cancer cells (15, 17, 18, 33–36). In the present study, we demonstrated that 2OHOA mediates the translocation of Ras from the plasma membrane to the cytoplasm as well as the subsequent inhibition of the MAP kinase (ERK, in vitro and in vivo) PI3K/Akt and Cyclin/CDK pathways (Fig. 3 and Fig. S4). In glioma cells, activation of the EGFR/Ras/Raf/ERK pathway blocks differentiation and induces the dedifferentiation of glial cells (11). Thus, inhibition of this signaling cascade constitutes a central event in the glioma-to-glial cell differentiation induced by 2OHOA, and it is most likely involved in 2OHOA-mediated cell cycle arrest and induction of autophagy.

2OHOA-induced PKC translocation to the membrane (and its concomitant activation) is associated with overexpression of the CDKI $p21^{Cip1}$ (4) and possibly of $p27^{Kip1}$ (Fig. S5), and with β-catenin downregulation (4, 19, 20). 2OHOA-induced overexpression of CDKIs and inactivation of cyclin D-CDK4/6 complexes (Fig. S5) is also associated with decreased Akt levels and RB phosphorylation (4, 37) and, therefore, with lower cell proliferation and reduced survival. Hypophosphorylation of RB prevents its dissociation from E2F-1 inhibiting the expression and activation of E2F-1, a pivotal transcription factor in cell cycle progression. These multiple regulatory effects probably contributed to glioma cell differentiation via inhibition of the MAPK-pathway as determined by the morphological (astroglial shape recovery) and molecular (increased expression of GS and GFAP) changes caused by 2OHOA, in vitro and in vivo.

We have shown in the present and previous studies (26) that the plasma membrane of glioma and all other cancer cells studied exhibit markedly low SM levels that appear to constitute a basic requirement to express the malignant phenotype. In the present study, we showed that 2OHOA induced recovery of SM levels and it was associated with potent effects against glioma. This fact suggests that remodeling of the membrane structure and composition would be upstream to the oncogenic action of Ras in cancer cells. Furthermore, this anticancer effect was associated with a dual-mode mechanism of action. On the one hand, the presence of 2OHOA in membranes and the increase in DAG would induce PKC translocation to membranes followed by CDKI overexpression and pRb hypophosphorylation (this work and refs. 4–6). On the other hand, Ras translocation to the cytosol would cause MAPK and Akt inactivation. These two pathways have been consistently seen to be involved in the loss of differentiation, increased proliferation, and survival of cancer cells so that their regulation by 2OHOA is most likely responsible for the induction of differentiation and autophagy observed upon treatment. In any case, additional molecular events/mechanisms should not be discarded. Indeed, we have recently seen that 2OHOA also induces marked increases in the levels of nuclear SM (26). In this context, nuclear phospholipids have been shown to participate in nuclear signaling and could account for some of the cellular effects induced by 2OHOA including glioma cell proliferation, differentiation and death (38).

Autophagy is an alternative program of cell death that may overcome the resistance of many cancers (e.g., glioma) to enter the apoptotic program (39). In this context, we detected that 2OHOA-induced autophagy in SF767 cells (Fig. 5). Thus, there were observed marked time and concentration dependent increases in the levels of ATG5 and LC3B, both proteins fundamental for the formation of autophagosomes (40). The induction of autophagy in glioma cells is triggered by RB hypophosphorylation and $p27^{kip1}$-mediated Akt inhibition (41) events induced by 2OHOA on these cells. In this context, the modifications in glioma cells caused by 2OHOA resulted in profound morphological changes, cell fragmentation, the release of cytosolic bodies containing ER cisternae, and an increase in lysosomes/autophagosomes, which is further evidence that autophagy is initiated. The high extent of autophagy in glioma cells upon treatment with 2OHOA specifically kills cancer but not nontumor cells and supports a recent hypothesis suggesting that autophagy might be used as a potential cancer therapy (42). The fact that autophagy occurred after induction of differentiation in SF767 cells treated with 2OHOA suggests that recovery of the features of mature cells may cause a molecular conflict to cancer cells. In contrast, neither autophagy nor the other molecular events here described were induced by 2OHOA in normal cells. This mechanism of action explains the extensive tumor cell death and lack of relapse

in animals treated with 2OHOA. Thus, 2OHOA is a first-in-class nontoxic membrane-lipid anticancer drug that activates sphingomyelin synthase and subsequently inhibits the MAPK and related oncogenic pathways.

Methods

Cells were incubated in DMEM (SF767) or RPMI 1640 (U118, A172 and T98G) in the presence of 10% FBS and antibiotics and in the presence or absence of 2OHOA or TMZ. Xenograft gliomas (subcutaneous and orthotopic) were developed in immunosuppressed mice by inoculation of SF767 cells. The data are expressed as the mean ± SEM values from 6–8 independent experiments or the number of animals indicated. Statistical significance was indicated: *, $P < 0.05$, **, $P < 0.01$, and ***, $P < 0.001$. Further details of the experiments are provided in the supporting information section.

ACKNOWLEDGMENTS. We are indebted to Prof. John E. Halver for his valuable ideas and suggestions. This work was supported by Grants BIO2010-21132, IPT-010000-2010-016 (Ministerio de Ciencia e Innovación, Spain), PROMETEO (Generalitat Comunitat Valenciana), and by the Marathon Foundation. S.T. and G.B.-C. were supported by Torres-Quevedo Research Contracts. M.L.M. and M.A.N.-S. were supported by fellowships from the Govern de les Illes Balears.

1. Brenner H, et al. (2009) Long-term survival expectations of cancer patients in Europe in 2000–2002. *Eur J Cancer* 45:1028–1041.
2. Louis DN (2006) Molecular pathology of malignant gliomas. *Annu Rev Pathol* 1:97–117.
3. Stupp R, et al. (2005) Radiotherapy plus concomitant and adjuvant temozolomide for glioblastoma. *New Engl J Med* 352:987–996.
4. Martínez J, et al. (2005) Membrane structure modulation, protein kinase Cα activation, and anticancer activity of Minerval. *Mol Pharmacol* 67:531–540.
5. Martínez J, et al. (2005) The repression of E2F-1 is critical for the activity of Minerval against cancer. *J Pharmacol Exp Ther* 315:466–474.
6. Lladó V, et al. (2009) Pivotal role of dihydrofolate reductase knockdown in the anticancer activity of 2-hydroxyoleic acid. *Proc Natl Acad Sci USA* 106:13754–13758.
7. Yung WK, et al. (1999) Multicenter phase II trial of temozolomide in patients with anaplastic astrocytoma or anaplastic oligoastrocytoma at first relapse Temodal Brain Tumor Group.. *J Clin Oncol* 17:2762–2771.
8. Omar AI, Mason WP (1999) Temozolomide: The evidence for its therapeutic efficacy in malignant astrocytomas. *Core Evid* 4:93–111.
9. Barceló F, et al. (2004) The hypotensive drug 2-hydroxyoleic acid modifies the structural properties of model membranes. *Mol Membr Biol* 21:261–268.
10. Goñi FM, Alonso A (1999) Structure and functional properties of diacylglycerols in membranes. *Prog Lipid Res* 38:1–48.
11. Harrisingh MC, Lloyd AC (2004) Ras/Raf/ERK signaling and NF1. *Cell Cycle* 3:1255–1258.
12. Katz M, Amit I, Yarden Y (2007) Regulation of MAPKs by growth factors and receptor tyrosine kinases. *Biochim Biophys Acta* 1773:1161–1176.
13. Griffero F, et al. (2009) Different response of human glioma tumor-initiating cells to epidermal growth factor receptor kinase inhibitors. *J Biol Chem* 284:7138–7148.
14. Wong ML, Kaye AH, Hovens CM (2007) Targeting malignant glioma survival signalling to improve clinical outcomes. *J Clin Neurosci* 14:301–308.
15. Kolch W (2000) Meaningful relationships: the regulation of the Ras/Raf/MEK/ERK pathway by protein interactions. *Biochem J* 351:289–305.
16. Leicht DT, et al. (2007) Raf kinases: function, regulation and role in human cancer. *Biochim Biophys Acta* 1773:1196–1212.
17. Parsa AT, Holland EC (2004) Cooperative translational control of gene expression by Ras and Akt in cancer. *Trends Mol Med* 10:607–613.
18. Tatevossian RG, et al. (2010) MAPK pathway activation and the origins of pediatric low-grade astrocytomas. *J Cell Physiol* 222:509–514.
19. Gwak J, et al. (2006) Protein-kinase-C-mediated beta-catenin phosphorylation negatively regulates the Wnt/beta-catenin pathway. *J Cell Sci* 119:4702–4709.
20. Gwak J, et al. (2009) Stimulation of protein kinase C-α suppresses colon cancer cell proliferation by down-regulation of beta-catenin. *J Cell Mol Med* 13:2171–2180.
21. Gartel AL, Tyner AL (2002) The role of the cyclin-dependent kinase inhibitor p21 in apoptosis. *Mol Cancer Ther* 1:639–649.
22. Marushige Y, et al. (1987) Modulation of growth and of morphological characteristics in glioma cells by nerve growth factor and glia maturation factor. *Cancer Res* 47:4109–4115.
23. Lee K, et al. (2005) Downregulation of GFAP, TSP-1, and p53 in human glioblastoma cell line, U373MG, by IE1 protein from human cytomegalovirus. *Glia* 51:1–12.
24. Leszczyniecka M, Roberts T, Dent P, Grant S, Fisher PB (2001) Differentiation therapy of human cancer: basic science and clinical applications. *Pharmacol Ther* 90:105–156.
25. Escribá PV (2006) Membrane-lipid therapy: a new approach in molecular medicine. *Trends Mol Med* 12:34–43.
26. Barceló-Coblijn G, et al. (2011) Sphingomyelin and sphingomyelin synthase (SMS) in the malignant transformation of glioma cells and in 2-hydroxyoleic acid therapy. *Proc Natl Acad Sci USA* 108:19569–19574.
27. Widemann BC, et al. (2011) Phase 1 trial and pharmacokinetic study of the farnesyl transferase inhibitor tipifarnib in children and adolescents with refractory leukemias: a report from the Children's Oncology Group. *Pediatr Blood Cancer* 56:226–233.
28. Mollinedo F, et al. (2010) Lipid raft-targeted therapy in multiple myeloma. *Oncogene* 29:3748–3757.
29. Modrak DE, Leon E, Goldenberg DM, Gold DV (2009) Ceramide regulates gemcitabine-induced senescence and apoptosis in human pancreatic cancer cell lines. *Mol Cancer Res* 7:890–896.
30. Escribá PV, et al. (1997) Role of lipid polymorphism in G protein-membrane interactions: nonlamellar-prone phospholipids and peripheral protein binding to membranes. *Proc Natl Acad Sci USA* 94:11375–11380.
31. Vögler O, et al. (2004) The G$\beta\gamma$ dimer drives the interaction of heterotrimeric Gi proteins with nonlamellar membrane structures. *J Biol Chem* 279:36540–36545.
32. Barceló F, et al. (2007) Interaction of the C-terminal region of the Ggamma protein with model membranes. *Biophys J* 93:2530–2541.
33. Guha A, Feldkamp MM, Lau N, Boss G, Pawson A (1997) Proliferation of human malignant astrocytomas is dependent on Ras activation. *Oncogene* 15:2755–2765.
34. Ohgaki H, Kleihues P (2009) Genetic alterations and signaling pathways in the evolution of gliomas. *Cancer Sci* 100:2235–2241.
35. Omerovic J, Laude AJ, Prior IA (2007) Ras proteins: paradigms for compartmentalised and isoform-specific signalling. *Cell Mol Life Sci* 64:2575–2589.
36. Holland EC (2000) A mouse model for glioma: biology, pathology, and therapeutic opportunities. *Toxicol Pathol* 28:171–177.
37. Kelly-Spratt KS, et al. (2009) Inhibition of PI-3K restores nuclear $p27^{Kip1}$ expression in a mouse model of Kras-driven lung cancer. *Oncogene* 28:3652–3662.
38. Irvine RF (2003) Nuclear lipid signalling. *Nat Rev Mol Cell Biol* 4:1–12.
39. Lefranc F, Facchini V, Kiss R (2007) Proautophagic drugs: a novel means to combat apoptosis-resistant cancers, with a special emphasis on glioblastomas. *Oncologist* 12:1395–1403.
40. Ferraro E, Cecconi F (2007) Autophagic and apoptotic response to stress signals in mammalian cells. *Arch Biochem Biophys* 462:210–219.
41. Jiang H, et al. (2010) The RB-E2F1 pathway regulates autophagy. *Cancer Res* 70:7882–7893.
42. Dalby KN, et al. (2010) Targeting the prodeath and prosurvival functions of autophagy as novel therapeutic strategies in cancer. *Autophagy* 6:322–329.

Supporting Information

Terés et al. 10.1073/pnas.1118349109

SI Text

Biomedical Relevance. The present study not only offers new possibilities for the treatment of glioma but also brings an innovative approach to overcome the therapeutic limitations in the treatment of various cancers. This work shows the proof of principle (efficacy in a humanized animal model of glioma) and proof of relevance (superiority with respect to any existing treatment) for a pathological process with unmet clinical needs. In addition, it is provided a comprehensive mechanism of action that covers from the first molecular events to the last cellular consequences of treatments with the synthetic fatty acid, 2-hydroxyoleic acid (2OHOA). Finally, this work provides relevant information about the use of GFAP, glutamine synthetase (GS), dihydrofolate reductase (DHFR), and sphingomyelin (SM) as potential biomarkers for the diagnosis of glioma and assessment of the therapeutic response and further indicates that sphingomyelin synthase (SMS) is a new anticancer drug target. The present results demonstrate that 2OHOA is a first-in-class compound.

As any other new discovery, the new knowledge brings numerous questions. First, further studies would be necessary to fully understand the molecular consequences of SM increases in the nucleus and plasma membrane. In addition, further investigation about molecular mechanism of interaction between PKC or Ras (two proteins whose cellular localization has been shown here to be altered by 2OHOA treatments) with bilayers of different SM and 2OHOA content. From the clinical point of view, and considering the current experience with 2OHOA in humans and animal models of cancer, it can be expected a full response to treatment in a significant proportion of cases from various types of cancers; however, the limited amount of data available makes it difficult to foresee the precise percentage of patients that could fully respond to treatment. In this scenario, it will be of great value to determine the molecular bases underlying full, partial, or no response upon 2OHOA treatment. In any case, the safety of this compound, its efficacy, its dual-mode mechanism of action, and the other data shown here suggest that in those cases that full response is not obtained, 2OHOA could be a very convenient companion in combination therapies using other drugs.

Finally, the signaling cascades covered in the present study are complex, and future studies would be required to shed further light on some of the molecular events here described. Thus, the induction of autophagy, which has been indicated to be related to the retinoblastoma protein phosphorylation status and the activities of Akt and $p27^{Kip1}$ (1), could imply intermediate states of ER stress. Most of these questions and additional issues of interest are currently under investigation in our laboratory. Nevertheless, only the results obtained in advanced phases of the clinical trials could determine the real relevance of this innovative compound. This specific and efficacious fatty acid, which constitutes the first member of a new family of anticancer compounds with no relevant toxicity at therapeutic doses, has a mechanism of action that presents several unusual features that had been indicated to be of potential interest in oncology (e.g., induction of differentiation and autophagy) (1, 2).

Extended Methods. ***Cell Lines and Culture.*** The human glioma cell lines U118, A172 and T98G were obtained from the European Collection of Human Cell Cultures, and SF767 cells were obtained from the Brain Tumor Research Center Tissue Bank (University of California-San Francisco, Department of Neurological Surgery). The cells were cultured at 37 °C in 5% CO_2 and DMEM (SF767) or RPMI 1640 (U118, A172 and T98G), supplemented with 10% fetal bovine serum (v/v), 100 units/mL penicillin, 0.1 mg/mL streptomycin, and 0.25 μg/mL amphotericin B. Media and other culture reagents were obtained from Sigma-Aldrich (Madrid, Spain).

Cell Proliferation Assays. Glioma cell growth was determined using the MTT (3-[4, 5-dimethylthiazol-2-yl]-2, 5- diphenyltetrazolium bromide) assay. Cells were cultured in 96-well plates at a density of $2.5 - 5 \times 10^3$ cells per well and incubated overnight. They were then incubated in the presence or absence of 2OHOA or temozolomide (TMZ) (concentrations and durations indicated in the figures) and, finally, in medium containing MTT (0.5 mg/mL, Sigma-Aldrich, Spain) for 2 h at 37 °C and 5% CO_2. Upon removal of MTT, 150 μl of DMSO was added to each well, and the absorbance was determined at 590 nm using a microplate reader (FLUOstar Omega, BMG LABTECH, Germany). To determine the correspondence between absorbance values and the number of viable cells, duplicate plates cultured in parallel under the same conditions but with increasing cell densities were counted using the trypan blue (0.2%) method.

Microscopy Studies. For confocal microscopy experiments, human glioma cells were cultured as indicated above in NUNC Lab-Tek II chambered slides (Nunc-Thermo Fisher Scientific, Denmark) and in the presence or absence of 2OHOA (150 μM, 10 min and 24 h), they were washed with Tris-buffered saline (TBS) buffer [137 mM NaCl, 2.7 mM, KCl, 25 mM, Tris-HCl (pH 7.4)] and fixed with 4% paraformaldehyde for 30 min at 4 °C. After washing twice with TBS buffer, cells were incubated with 5% normal horse serum in TBS buffer for 1 h at room temperature and then immediately incubated overnight at 4 °C with a monoclonal anti-Ras antibody (1:50, BD Transduction Laboratories, Heidelberg, Germany) in TBS buffer supplemented with 2% horse serum. Finally, the cells were washed with TBS buffer, incubated for 1 h with the secondary antibody (Alexa Fluor 488-labeled goat anti-mouse IgG, 1:200, Molecular Probes; excitation at 488 nm and detection at 510–550 nm), and washed with TBS buffer. Images were acquired on a Leica TCS SP2 spectral confocal microscope with 630x optical magnification and 8x digital magnification (approximately 5,000x total magnification), and they were analyzed with the manufacturer's software. To detect lysosomes, cells were cultured as above in the presence or absence of 2OHOA or palmitate (150 μM, 48 hours). The cells were then incubated for 1 h with the LysoSensor Green DND-189 probe pH Indicator (2 μM, pH 4.5–6, Invitrogen) to detect autophagosomes, and for 5 min with Hoecht 33342 (trihydrochloride trihidrate, 40 μg/mL, Invitrogen), to stain the nuclei. Samples were observed on a Nikon Eclipse TE2000-S fluorescence microscope at 400x magnification. The fluorescence induced by the acidic vesicles was quantified in photomicrographs of live cells using Image J 1.38x public software (Wayne Rasband, National Institutes of Health; rsb.info.nih.gov).

Electron microscopy experiments were performed in triplicate and, for each incubation time and concentration used, a total of 300 control or treated cells were analyzed giving a total of 3600 cells. For this purpose, SF767 cells were seeded at a density of 4×10^4 cells/well in 4-well Lab-Tek chamber slides (Nalge Nunc Int., Naperville, IL) and fixed in 3.5% glutaraldehyde for 1 h at 37 °C. The cells were then postfixed in 2% OsO_4 for 1 h at room temperature and stained with 2% uranyl acetate in darkness for 2 h at 4 °C. Finally, cells were rinsed in 0.1 M sodium phosphate buffer (pH 7.2), dehydrated in ethanol, and infiltrated overnight with

Araldite (Durcupan, Fluka, Buchs SG, Switzerland). Following polymerization, embedded cultures were detached from the chamber slide and glued to araldite blocks. Serial semithin (1.5 μm) sections were cut with an Ultracut UC-6 microtome (Leica, Heidelberg, Germany), mounted onto slides, and stained with 1% toluidine blue (optical microscopy). Selected sections were glued (Super Glue, Loctite) to araldite blocks and detached from the glass slide by repeated freezing (in liquid nitrogen) and thawing. Ultrathin (0.06–0.09 μm) sections were prepared on the Ultracut microtome and stained with lead citrate. Finally, photomicrographs were obtained using a transmission electron microscope (FEI Tecnai G2 Spirit Biotwin) coupled to an Olympus digital camera.

Electrophoresis, Immunobloting and Protein Quantification. Cells were cultured in 6-well plates at a density 1.5×10^5 cells per well. After incubation in the presence or absence of 2OHOA at the indicated concentrations and times, 150 μl of protein extraction buffer [10 mM Tris-HCl (pH 7.4)] containing 50 mM NaCl, 1 mM $MgCl_2$, 2 mM EDTA, 1% SDS, 5 mM iodoacetamide, and 1 mM PMSF) was added to each well. The contents of two wells were subjected to identical treatments, pooled, and further processed. Cell suspensions were subjected to ultrasound (70% cycle) for 10 s at 50 w using a Braun Labsonic U (probe-type) sonicator, and 30 μl aliquots were prepared for protein quantification. For PKC translocation experiments, this cell suspension was subsequently centrifuged as described elsewhere (3) and PKCα levels were determined by immunoblotting in the membrane and cytosolic fractions.

Tumors derived from immunosuppressed mice injected with SF767 cells were frozen in liquid nitrogen and ground in a glass mortar. The resulting powder was homogenized using a tissue blender (Ultra-Turrax; Janke & Kunkel) in ice-cold protein extraction buffer (1:10 w/v). The homogenate was incubated for 30 min at room temperature and then subjected to ultrasound as described above. Samples were centrifuged for 15 min at 1,000×g and 4 °C, and 30-μl aliquots of the resulting supernatant was used to determine the total protein content. The remaining volume (about 270 μl) was mixed with 30 μl of 10 x electrophoresis loading buffer [120 mM Tris-HCl (pH 6.8)], 4% SDS, 50% glycerol, 0.1% bromophenol blue, and 10% β-mercaptoethanol) and boiled for 3 min.

For immunoblotting, 30 μg of total protein from the cell lysates was resolved by SDS polyacrylamide gel electrophoresis (SDS-PAGE) and transferred onto nitrocellulose membranes (Schleicher & Schüell). After immunoblotting, nitrocellulose membranes were blocked for 1 h at room temperature in TBS containing 5% nonfat dry milk and 0.1% Tween 20 (blocking solution). The membranes were then incubated overnight at 4 °C in blocking solution containing one of the following primary antibodies: anti-Ras, anti- MAP kinase kinase (anti-MEK), anti-MEKP, anti-extracellular, signal-regulated kinase (anti-ERK), anti-ERKP, antiepidermal growth factor receptor (anti-EGFR), anti-EGFRP, anti-$p21^{Cip1}$, anti-LC3B, anti-Atg5, anti-Raf or anti-RafP (1:1000, Cell Signaling, Danvers, MA); anti-PKC, anti-Cyclin D3, anti-E2F1 (1:1.000, BD Transduction Laboratories, Heidelberg, Germany); anti-GFAP, anti-$p27^{Kip1}$ (1:1000, Abcam, Cambridge, UK); anti-glutamine synthetase (1:2000, Amersham, Billerica, MA); and anti-α tubulin (1:14,000, Sigma-Aldrich, St. Louis MO). After incubation with the primary antibody, membranes were washed three times for 10 min with TBS and incubated for 1 h at room temperature in fresh blocking solution containing horseradish peroxidase-linked goat anti-mouse or donkey anti-rabbit IgG (1:2,000, Amersham Pharmacia). Antibody binding (i.e., protein level quantification) was assessed by Enhanced Chemiluminescence Detection (ECL; Amersham Pharmacia) followed by exposure to ECL hyperfilm (Amersham Pharmacia). The α-tubulin content in the samples was determined by the same procedure and used as a loading control. The films were scanned at a resolution of 600 dpi (41.6 μm resolution), and problem sample bands were interpolated in standard curves of integrated optical density vs. protein content to quantify the relative levels of a given protein with reference to four control samples of different protein content loaded on the same gel. The concentration measured for a given protein was divided by the α-tubulin content of the same sample. The results shown in SF767 cells correspond to mean ± SEM values from triplicate samples measured in 6–8 independent experiments (for a total of 18–24 measurements for each protein). For studies in mouse tumors, the number of animals used is indicated in the corresponding section.

Membrane Lipid Analysis. Cell membrane lipids were extracted directly from the frozen monolayer of cells using the n-hexane: 2-propanol (3:2, v/v) extraction method with slight modifications. Briefly, SF767 cells were cultured as described above and maintained for 72 h in the presence or absence or 2OHOA (200 μM). Frozen cells were washed with PBS, lipids were extracted by the direct addition of 2.2 mL of 2-propanol, and the cells were subsequently removed from the plate using a Teflon cell scraper. The total protein concentration was then determined using the bicinchoninic acid assay (Thermo scientific, Rockford). Then, 6 mL of hexane was added to the mixture and removed. The cell dish was rinsed with another 2.2 mL of 2-propanol that was combined with the first hexane/2-propanol mixture. Cell extracts were then centrifuged at 1000×*g*, and the pellet containing denatured proteins and other cellular debris was discarded. The lipid-containing organic phase was decanted and stored under a N_2 atmosphere at −80 °C until analysis. Individual phospholipid classes and neutral lipids were separated by thin layer chromatography (TLC) or (high performance) thin layer chromatography [(HP) TLC], respectively, on Whatman silica gel-60 plates (20 × 20 cm, 250 μm or 10 × 10 cm, respectively) that were heat-activated at 110 °C for 1 h, and the samples were streaked onto the plates. Phospholipids were separated using chloroform/methanol/acetic acid/water (55:37.5:3 : 2 v/v/v/v), and the phospholipid mass was determined by measuring the lipid phosphorus content of individual lipid classes separated by TLC. Neutral lipids were separated in petroleum ether/diethyl ether/acetic acid (75:25 : 1.3 v/v/v), and the lipid fractions were identified using lipid standards (Larodan, Sweden). After development, plates were air dried, sprayed with 8% (w/v) H_3PO_4 containing 10% CuSO4 (w/v), and charred at 180 °C for 10 min. Lipids were then quantified by image analysis.

Near Infrared Spectroscopy Immunofluorescence. For some immunocytochemical studies, mouse tumors ($N = 10$) were fixed with 4% paraformaldehyde in 100 mM phosphate buffer (pH 7.4), embedded in paraffin, and sections were cut serially (7 μm) using a microtome. Tissue sections were deparaffinized with xylene, and they were rehydrated with ethanol. The sections were then placed in an antigen retrieval solution (Dako A/S, Glostrup, Denmark) for 10 min at 95 °C and rinsed in 100 mM Tris-buffered saline (pH 7.4, TBS). Subsequently, the sections were incubated for 1 h in TBS containing 0.1% Triton X-100 and 5% horse serum followed by overnight incubation at 4 °C with a specific primary antibody against human GFAP (1:100, Abcam, Cambridge, UK). Following four 15 min washes with TBS containing 0.05% Tween 20 (TBST), the tissue sections were incubated for 1 h at room temperature with IRDye™ 800CW-conjugated donkey anti-rabbit IgG (1:8,000, Li-Cor, Lincoln, Nebraska) in blocking solution. The tissue sections were washed four times in TBST. Following a brief rinse with water, sections were allowed to air dry for at least 1 h before fluorescence was detected using the Li-Cor Odyssey Near Infrared Scanner (21 μm resolution, 1 mm offset with highest quality). Channel sensitivity was optimized for each set of stained sections, and the tumor areas were

defined and the integrated intensities were determined with Odyssey software.

In addition to the above ex vivo measurements, in vivo determination of glutamine synthetase expression was performed by near infrared spectroscopy. Accordingly, IRDye 800CW was covalently bound to an anti-glutamine synthetase antibody (Abcam) using the reagents provided by the manufacturer (High MW protein labeling kit, Li-Cor). For in vivo determinations of this enzyme, nude mice were infected with SF767 cells except that the treatments (p.o., 600 mg/kg 2OHOA or 80 mg/kg TMZ or vehicle; $N = 10$ per group) commenced 15 d after cell inoculation and lasted only seven days. IRDye 800CW-anti-glutamine synthetase (50 μg) was then injected intravenously through the tail vein and fluorescence was acquired in vivo using the Li-Cor Odyssey Near Infrared Scanner at 72–144 h postinjection. During this postinjection time (144 h), treatments were maintained as above.

Animals, Tumor Grafts and Treatments. Male NUDE (Swiss) Crl:NU (Ico)-Foxn1^{nu} mice (five week-old, 30–35 g, Charles River Laboratories, Paris, France) were maintained in a thermostat cabinet (28 °C, EHRET, Labor-U-Pharmatechnik) with a sterile air flow at a relative humidity of 40–60% and a 12 h dark/light cycle.

For xenograft tumors derived from human glioma (SF767) cells, 7.5×10^6 cells were inoculated subcutaneously into the animal dorsal area and after one week, tumors were already visible. Animals were randomly divided into groups with a similar mean tumor volume, and they received daily oral treatments with the vehicle alone (water), 2OHOA (600 mg/kg, except in the dose-dependence studies), TMZ (80 mg/kg), or 2OHOA + TMZ (same doses) for 50 ($N = 20$ per group, line graphs in Fig. 1) or 60 days ($N = 15$ per group, bar graphs, line graphs in Fig. 1). In vivo near infrared studies ($N = 10$) and studies of the efficacy of the free acid or the salts ($N = 5$) were performed over seven and 14 days, respectively. Tumor volumes were calculated as $v = w^2 \times L/2$ where w is the tumor width and L its length.

After the final tumor volume measurements, mice were sacrificed by decapitation, the tumors were removed and immediately frozen in liquid nitrogen before being stored at 80 °C for molecular studies or maintained in 10% formaldehyde for histological studies. All experiments were carried out in accordance with the animal welfare guidelines of the European Union and the Institutional Committee for Animal Research of the University of the Balearic Islands.

For orthotopic SF767 grafts in nude mice, cells were collected from cultures at 80% confluence, resuspended in PBS containing 0.05% trypsin and 0.02% EDTA, and centrifuged at $600 \times g$ for 5 min at room temperature. Cell pellets were then resuspended in fresh culture medium and rapidly counted in a Burker chamber. After a second centrifugation in the same conditions, the cells were resuspended in serum-free medium and used to infect mice. Male NUDE (Swiss) Crl:NU(Ico)-Foxn1^{nu} mice were anesthetized with ketamine (60 mg/kg, i.p.) and diazepam (7.5 mg/kg, i.p.). Animals received approximately 3×10^5 SF767 cells (>90% viability) in a volume of 3 μl stereotactically injected in the right caudate nucleus: bregma (anatomical point on the mouse skull at which the coronal suture is intersected perpendicularly by the sagittal suture) 0.5 mm; lateral, 1.75 mm. The needle was initially advanced to a depth of 4 mm and then withdrawn to a depth of 3 mm to limit reflux up the needle tract during injection of cells. After six weeks, the animals were anesthetized and perfused with 4% paraformaldehyde in phosphate buffered saline to fix the brain. Vibratome sections (50 μm) were obtained and immunochemical detection was performed using the HuNu antibody [Millipore, 1:400) and the biotin-avidin-peroxidase complex method (Vector)] visualizing the antibody binding with diaminobenzidine (DAB; Vector). For each animal, quantitative estimates of the total number of grafted cells were determined stereologically using the optical fractionator. The rostral and caudal limits of the reference volume were determined from the first and last frontal sections that contained grafted cells. The sample sites were systematically and automatically generated by the computer and examined using a 60x objective on a Nikon Eclipse TE 300 microscope.

Data Analysis. The data are expressed as the mean ± SEM values from 6–8 independent experiments involving triplicate samples and the number of animals indicated. Experimental groups were compared using one-way ANOVA followed by the Bonferroni multiple-comparison test or the two-tailed t test where appropriate. The differences between experimental groups were considered statistically significant at $P < 0.05$. For statistical significance was also taken as $^*P < 0.05$, $^{**}P < 0.01$, and $^{***}P < 0.001$.

1. Jiang H, et al. (2010) The RB-E2F1 pathway regulates autophagy. *Cancer Res* 70:7882–7893.
2. Leszczyniecka M, Roberts T, Dent P, Grant S, Fisher PB (2001) Differentiation therapy of human cancer: Basic science and clinical applications. Pharmacol Ther 90:105–156.
3. Martínez J, et al. (2005) Membrane structure modulation, protein kinase C alpha activation, and anticancer activity of Minerval. *Mol Pharmacol* 67:531–540.

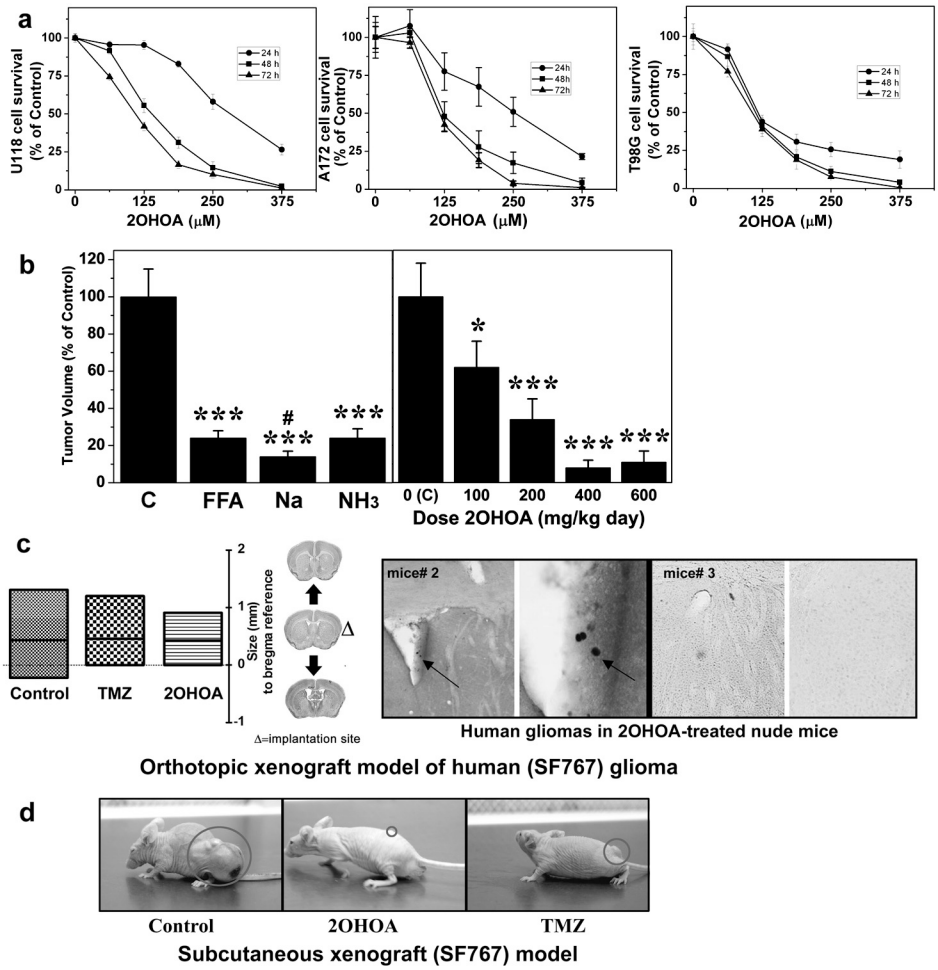

Fig. S1. (*A*) Efficacy of 2OHOA against various types of human glioma cells. Time and concentration dependent inhibition of human glioma cells (U118, *left*; A172, *center*; T98G, *right*) by 2OHOA. (*B*), Effects of the vehicle alone (control, *C*), the free fatty acid form of 2OHOA (FFA), and the sodium (Na) and ammonium (NH_3) salts of 2OHOA, on the SF767-derived tumor volume after 14 days of treatment (600 mg/kg, p.o., $N = 5$). Dose-response effect of 60-day 2OHOA treatment (second graph, $N = 10$). *$P < 0.05$, ***$P < 0.001$, with respect to Control; #, $P < 0.05$ with respect to other treatments. (*C*), Distribution of $HuNu^+$ cells in the brain of mice (*left*, mm to bregma reference, orthotopic model). Additional images showing the effect of oral 2OHOA treatment on the brain of nude mice infected with human glioma cells (*right* panels). In one of the mice (number 2) only a few glioma cells remained (*arrows*); whereas, in the other three mice (mice number 3 is shown as an example) no glioma cells remained. $N = 5$ for all experimental groups. (*D*), Representative photographs of mice infected with SF767 cells and treated with the vehicle alone (Control), 2OHOA (600 mg/kg, p.o., 60 days), and TMZ (80 mg/kg, p.o., 60 days).

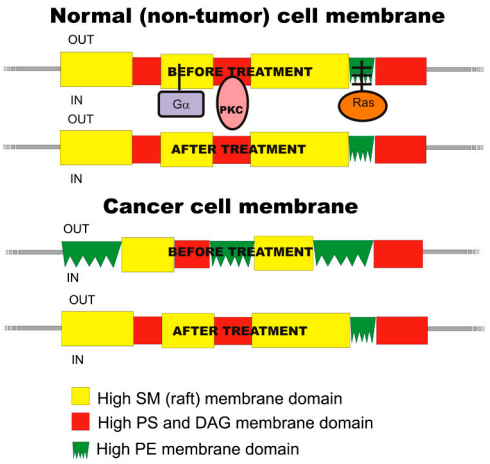

Fig. S2. *Upper Scheme*, Distribution of the distinct membrane domains in normal cells and examples of proteins bound to SM-rich (yellow), diacylglycerol (DAG)-rich (red), and phosphatidylethanolamine (PE)-rich (green) membrane microdomains before and after treatment with 2OHOA. *Lower Scheme*, Distribution of microdomains in glioma (and other cancer) cells before and after 2OHOA-induced increases in SM and DAG and decreases in PE.

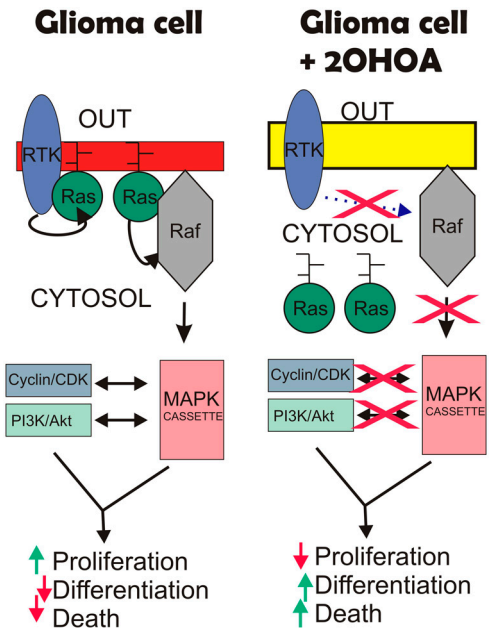

Fig. S3. Scheme of Ras-associated signaling in human glioma cells before (*left*) and after treatment with 2OHOA (*right*). Signals that induce cell proliferation, loss of differentiation, and survival are often propagated through Receptor Tyrosine Kinases [(RTK), e.g., EGFR] that activate Ras that in turn activates Raf. Then, Raf activates MEK, which finally phosphorylates and activates mitogen-activated protein kinase (MAP kinase). The Ras/MAPK signaling cassette regulates positively the PI3K/Akt and Cyclin/CDK pathways. In the presence of 2OHOA, Ras translocates to the cytoplasm, which prevents RTK-Ras and Ras-Raf interactions that only occur at the plasma membrane and impairs the signaling and cross-talk events mentioned above.

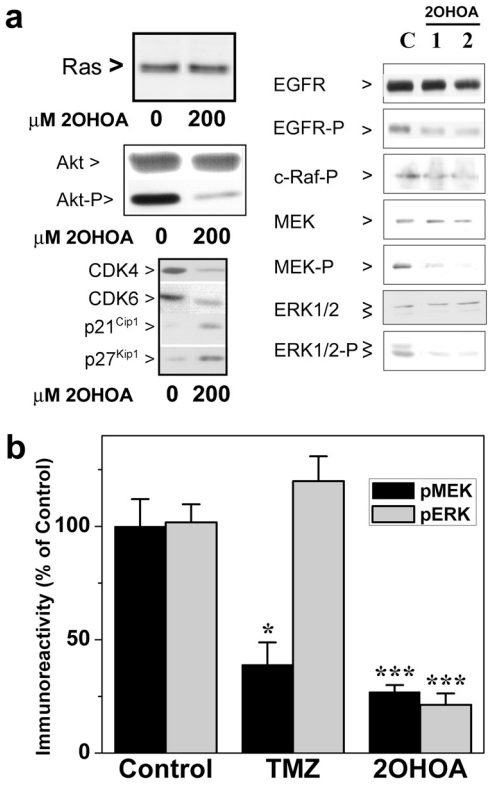

Fig. S4. *A*), Representative immunoblots of the various proteins (or phosphoproteins, -P) whose levels have been quantified in SF767 cells treated in the presence or absence (control, *C*) of 150 (1) or 200 μM (2, 200) 2OHOA (see Figs. 3 and 4 in the main text). (*B*), Effect of 2OHOA on the levels of phospho-MEK and phospho-ERK in SF767-derived tumors. Nude mice bearing tumors were treated with vehicle, TMZ (80 mg/kg, p.o., daily) or 2OHOA (600 mg/kg, p.o., daily) for 50 d. Then, animals were killed and the levels of these proteins measure by quantitative immunoblotting.

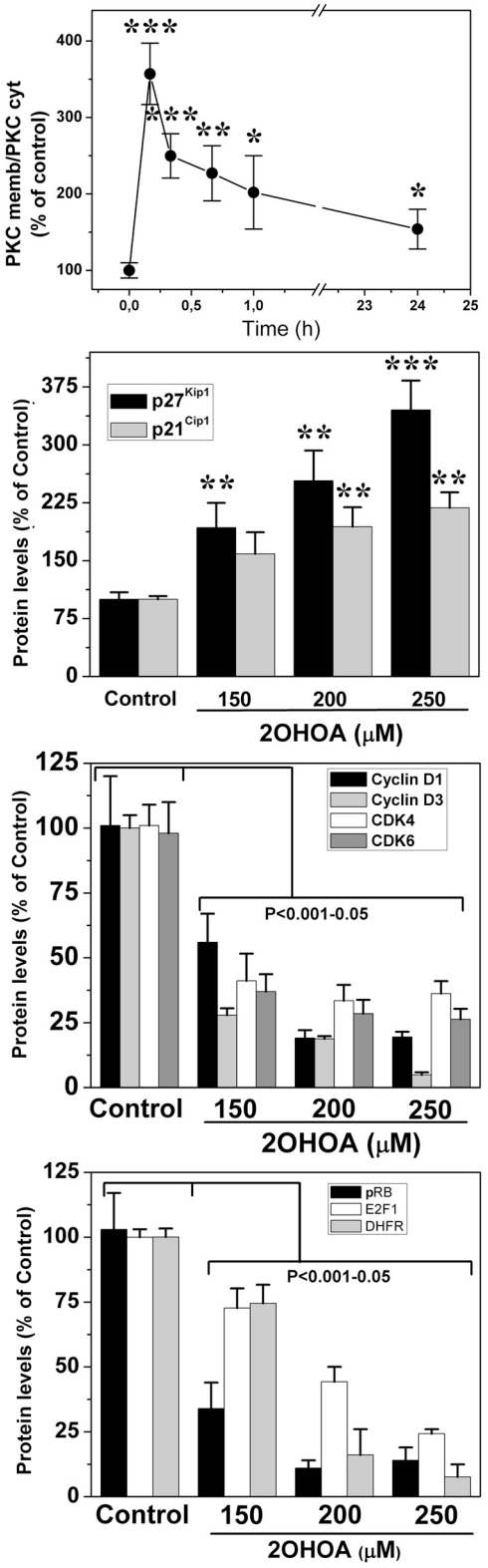

Fig. S5. Effects of 2OHOA on cell (SF767) cycle proteins. *Upper panel*: Incubation with 2OHOA (200 μM) for varying lengths of time induces PKCα translocation to the membrane (ratio of membrane to cytosolic PKCα, as determined by quantitative immunoblotting. Effects of 2OHOA treatment (48 h at the concentrations indicated) on $p21^{Cip1}$ and $p27^{Kip1}$ (*second panel*), Cyclin D1, Cyclin D3, CDK4 and CDK6 (*third panel*), and (*C*) Effect of 2OHOA (48 h at the concentrations indicated) on phosphorylation of the retinoblastoma protein (pRB/RB ratio), E2F-1 and DHFR (*bottom panel*). Quantitative immunoblotting ($N = 6$–8) was used in all cases.

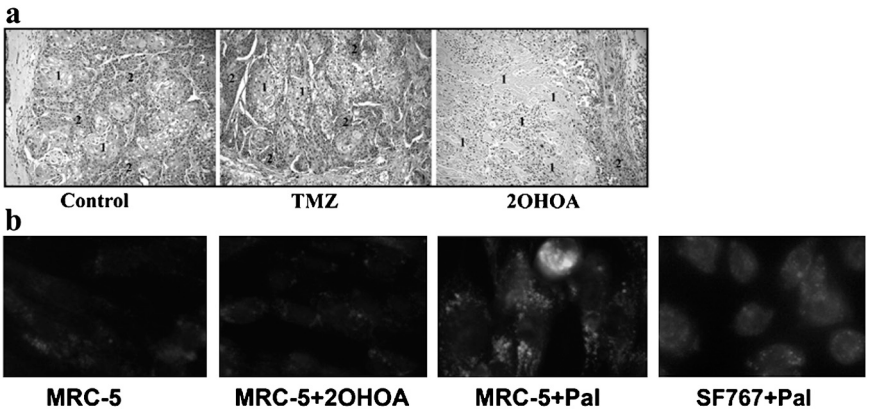

Fig. S6. 2OHOA induces tumor cell death, in vivo, and ER stress-autophagy, in vitro. (*A*) Hematoxylin-eosin staining of tumor sections from mice treated with the vehicle alone (Control), TMZ (80 mg/kg, p.o., 50 d) or 2OHOA (600 mg/kg, p.o., 50 d), showing areas with dead (1) and living (2) cells. (*B*) Fluorescence microscopy of lysosomes/autophagosomes labeled with Lysosensor in nontumor MRC-5 cells in the presence or absence (MRC-5) of 2OHOA (MRC − 5 + 2OHOA: 150 μM for 48 h) or palmitic acid (MRC − 5 + Pal, 150 μM for 48 h). The effects of Pal on SF767 is also shown (SF767 + Pal). Palmitic acid is a known inducer of ER stress and autophagy. $N = 400$ cells from five independent experiments.